IMPROVED EVALUATION OF LAYER CHARGE OF *n*-ALKYLAMMONIUM-TREATED FINE SOIL CLAYS BY LORENTZ- AND POLARIZATION-CORRECTION AND CURVE-FITTING

H. STANJEK, E. A. NIEDERBUDDE AND W. HÄUSLER

Lehrstuhl für Bodenkunde der Technischen Universität München, Freising-Weihenstephan, Germany

(*Received 25 February 1991; revised 10 June 1991*)

ABSTRACT: The clay mineralogy of K-fixing soils from southern Germany was investigated using the alkylammonium method. Conventional X-ray diffraction chart recordings of glycerol-saturated <0·1 μm samples showed peaks at 18 Å that were initially interpreted as smectites. However, step-scanning combined with the Lorentz- and polarization-correction and curve-fitting, revealed the presence of low- and high-charge smectites and of low- and high-charge vermiculites. The severe overlap of the 001 basal reflections of the high-charge vermiculites with the broad and intensive peaks of smectites *sensu stricto* prevented visual evaluation at the alkylchains n_c = 5–9, but this problem was overcome by curve-fitting. The 002 peaks of high-charge vermiculites (n_c = 8 and n_c = 10) in the fraction 0·1–0·2 μm could furthermore be clearly resolved from the 001 peaks of illite by curve-fitting. In one example, 003 (at n_c = 17) could be resolved from 001 of illite.

Clay minerals exert a marked influence on the physical and chemical properties of soils such as shrinking and swelling behaviour or adsorption and desorption of nutrient elements. Their precise characterization is therefore essential for the understanding of major soil properties. The formation of interlayer complexes with glycerol or ethylene glycol (Walker, 1958; Brindley, 1966) allows distinction between expandable and non-expandable clay minerals, but gives no evidence on the layer charge. Direct measurements of the layer charge using alkylammonium ions were first carried out on pure, well-crystallized smectites and vermiculites (Lagaly & Weiss, 1969, 1976; Lagaly, 1982). Later a modified procedure was applied to soil and sediment clays (Rühlicke & Niederbudde, 1985; Malla & Douglas, 1987; Laird *et al.*, 1988, 1989; Ghabru *et al.*, 1989; Chen *et al.*, 1989); in all of these papers, X-ray diffraction (XRD) diagrams were evaluated by visual inspection.

In contrast to clay minerals from economic deposits, soil clays (especially the finer fractions) yield XRD diagrams of "poorer" quality because of broadened and overlapping peaks (cf., Weir & Rayner, 1974). This results in shifts of the peak maxima and is furthermore accompanied by an inevitable peak distortion due to the increasing background intensity towards lower angles. The considerable inaccuracy arising from visual evaluation can, however, be reduced substantially by step-scanning combined with a correction for the Lorentz- and polarization-factor and subsequent curve-fitting (Stanjek & Friedrich, 1986). The improved determination of peak positions—when calibrated against an internal standard, for instance talc (Häusler & Stanjek, 1988)—gives more reliable information on the properties of soil clay minerals and is applicable to transformation processes during mineral weathering or the K-fixing behaviour of soil clay minerals.

The purpose of this investigation was to compare the evaluation of uncorrected and

corrected XRD diagrams and to discuss the consequences for the layer charge determination of sheet-silicates. Smectite (*sensu stricto*), high-charge vermiculite, and vermiculite with charge heterogeneity (Lagaly, 1982) occurring in the same sample also had to be distinguished. A further objective of this study was to evaluate the usefulness of the 002 peak evaluation of alkylammomium-treated soil vermiculite, which is made possible by correction of the XRD diagram for the Lorentz- and polarization-factor (Lp), and use of curve-fitting. To study the particle size effect, two soil clay fractions were chosen.

MATERIALS AND METHODS

The fractions <0·1 μm and 0·1–0·2 μm were separated from three soils from southern Germany. Samples #1 (<0·1 μm) and #4 (0·1–0·2 μm) are from a Würm II loess (Udalf, 95–110 cm), #2 (<0·1 μm) and #5 (0·1–0·2 μm) are from the Ap horizon of an Aquept (0–25 cm, alluvial soil of a K_0 plot from a long-term fertilizer experiment), and #3 and #6 (0·1 μm and 0·1–0·2 μm) are from the Go horizon (30–40 cm) of a Humaquept (alluvial soil). The total clay contents vary between 22 and 45%, with high proportions of fine clay (50–60% <0·2 μm, 35–45% <0·1 μm). Potassium fixation of the selected soils ranged from 43 to 79% of added K (10 mg K/g clay). The rather high K fixation is also reflected in the low AR_0 values of 5×10^{-4} down to 5×10^{-5} $M^{\frac{1}{2}}$, which were calculated from K-Ca exchange curves (Beckett, 1964).

Clay fractions (<0·1 μm and 0·1–0·2 μm) were separated by gravitational settling and centrifugation after removing organic matter with H_2O_2, and free iron oxides with dithionite-citrate-bicarbonate (Mehra & Jackson, 1960). The samples were Ca-saturated by adding 1 N $CaCl_2$ and then washed free of excess salts. To determine the layer-charge density, the freeze dried samples were treated with *n*-alkylammonium chloride (n_c = 5–17 or 18) following the procedure of Rühlicke & Niederbudde (1985). Samples 2–6 were prepared for XRD with talc as an internal standard (Häusler & Stanjek, 1988). A semi-quantitative characterization of the Ca-saturated clays after glycerol treatment was carried out using the following intensity correction factors: 0·23 for kaolinite (*d*-value 7 Å), 0·34 for vermiculite (14 Å), 0·25 for smectite (18 Å) and 1·0 for illite (10 Å). These factors are mean values of several studies (Gjems, 1967; Laves & Jähn, 1972; Niederbudde & Kußmaul, 1978).

EXPERIMENTAL PROCEDURES

Data collection and processing

A Philips PW 1070 diffractometer with Co radiation (λ = 1·79026 Å) and diffracted beam monochromator was equipped with a digital data output device. The output, stored in a commercial printer buffer, was read out into an IBM-compatible computer via the serial interface by a program (written in Turbo-Pascal) and stored in an appropriate format on a disk.

Lorentz- and polarization-correction

Included within the data collecting program is a routine for the Lorentz- and polarization-correction (Stanjek & Friedrich, 1986), which divides the counts by the Lp factor (taken from Klug & Alexander, 1973):

$$Lp = \frac{1 + \cos^2 2\theta}{\sin^2\theta\cos\theta}$$

and multiplies them with a constant factor of ~1000 to adjust the intensities to their original level.

Smoothing of raw data

It is often necessary to smooth X-ray data to improve the quality of the scan. We used smoothing procedures based either on a polynomial algorithm published by Savitzky & Golay (1964, 1972) or on weighting functions based on a program written by Hilberg (1989). The latter program allows the weighting of the data according to their counting statistics. Sharp and intense peaks are smoothed near the baselines but are less (or not) affected at the tops of the peaks. This diminishes the reduction and distortion of sharp peaks when using polynomial functions.

Fitting of the X-ray scans

In fine soil clays, peaks are broadened as a result of the small particle size (Scherrer, 1918). Peak overlap not only shifts maxima to lower or higher angles, but prevents the evaluation of precise positions. Curve-fitting programs, amply available now (for the state of the art see Bish & Post, 1989), can resolve overlapping peaks and substantially increase the precision of evaluation (cf., Stanjek & Friedrich, 1986). The curve-fitting program FIT, originally developed by Janik & Raupach (1977) for IR spectra and later adapted to fit XRD data (Schulze, 1984), simultaneously optimizes positions, heights, widths at half-height (WHH), the (linear) baseline and varying ratios of Gaussian and Cauchy peak shapes (Pseudo-Voigt function) by an iterative least-squares method for up to 16 peaks. The program needs an input of preliminary estimates of all parameters, which are taken from visual evaluations of plots of the Lp-corrected X-ray diagram. The fitting progam adjusts all parameters to minimize the deviations between the actual scan and the calculated sum of all entered peaks (referred to as the envelope). After convergence, i.e. when no further significant reduction in the coefficient of variation takes place, the program displays the estimated best parameters of all peaks together with an estimate of the baseline and the Gauss/Cauchy ratio.

Correction and calculation of precise d-values

The program FITKORR (TurboPascal) first corrects the angles 2θ for non-linear behaviour of the goniometer using a calibration function established with hexadecanol (Brindley, 1981). The 2θ angles are then corrected against the position of the internal standard talc (samples 2–6) to improve precision, and converted into d-values (Häusler & Stanjek, 1988).

Calculation of the layer charge

Smectites. The transition from the monolayer to the bilayer arrangement of alkyl chains was used to calculate the layer-charge distribution of smectites (Lagaly *et al.*, 1976). Short chains (small n_c) yield d-values of ~13·6 Å (i.e. the monolayer), whereas longer chains yield d-values of ~17·7 Å (bilayer arrangement).

TABLE 1. Mineral quantities (in wt% after glycerol saturation) and potassium release with $n_c = 18$.

Fraction	Sample no.	*d*-value (Å) 18	14	10	7	Kt (%)*	K extracted by n_c 18 (cmol/g)	(% of Kt)
	1	82	0	15	3	1·6	3·84	9·4
<0·1 μm	2	81	0	16	2	1·6	3·02	7·4
	3	98	0	2	0	1·0	1·53	6·0
	4	28	38	22	12	1·8	6·83	14·8
0·1–0.2 μm	5	30	35	19	15	2·0	10·38	20·3
	6	65	21	8	6	1·4	4·22	11·8

* total potassium.

High-charge vermiculites. High-charge vermiculites are identified by a linear increase of d_{001} (or d_{002}) with increasing chain length. The layer charge can be calculated from the slope of the regression line of $\Delta d/\Delta n_c$ (Lagaly *et al.*, 1976). In order to minimize the confidence limits of the calculated layer charges, the correlation coefficient of the regression should be as close to unity as possible (Stanjek & Friedrich, 1986; Häusler & Stanjek, 1988).

Low-charge vermiculites. For low-charge vermiculites ($\xi < 0{\cdot}7$) the transitions between 17·7 Å (at $n_c \approx 6$–9) and 21·7 Å (at $n_c \approx 13$–17) were used to estimate the layer charge. These transitions are similar to the Beni-Buxera, Young River and South Africa types (cf. Fig. 3 and Fig. 4 in Lagaly, 1982).

RESULTS AND DISCUSSION

A quantitative phase analysis of glycerol-saturated samples showed remarkable differences between the fractions <0·1 μm and 0·1–0·2 μm of all three soils. The fraction <0·1 μm is dominated by 18 Å expandable minerals (smectites *sensu lato*), whereas 14 Å phases are absent and the proportions of illite (10 Å) range from 2 to 16%. Traces of kaolinite were also detected (Table 1, Fig. 1). In the fraction 0·1–0·2 μm, however, the 18 Å phases are significantly depleted relative to 14 Å phases, which contract with K to 10 Å. Traces of chlorite were detected in soils 2 and 3 (samples 4 and 5). The illite contents are slightly higher than in the finer fraction, whereas the kaolinite contents increase substantially up to 15% (Table 1).

The total K contents of all samples (Table 1) do not agree with the illite contents determined by XRD. Assuming a minimum of 6·5% K in illite (lowest value cited by Reynolds, 1980, p. 276), the illite contents have been underestimated. This may possibly be due to the partial overlap of the second-order peak of the expanded 10 Å phase with 001 of illite, which hampered the visual evaluation of the illite peak area (cf. Fig. 1). An alternative explanation is that small amounts of illite could be randomly interstratified with smectite layers.

Comparison of uncorrected with Lp-corrected X-ray diagrams

The effect of the Lorentz- and polarization-correction upon the apparent *d*-values and intensities is depicted in Fig. 2 for the alkylammonium-treated fraction <0·1 μm of sample 1.

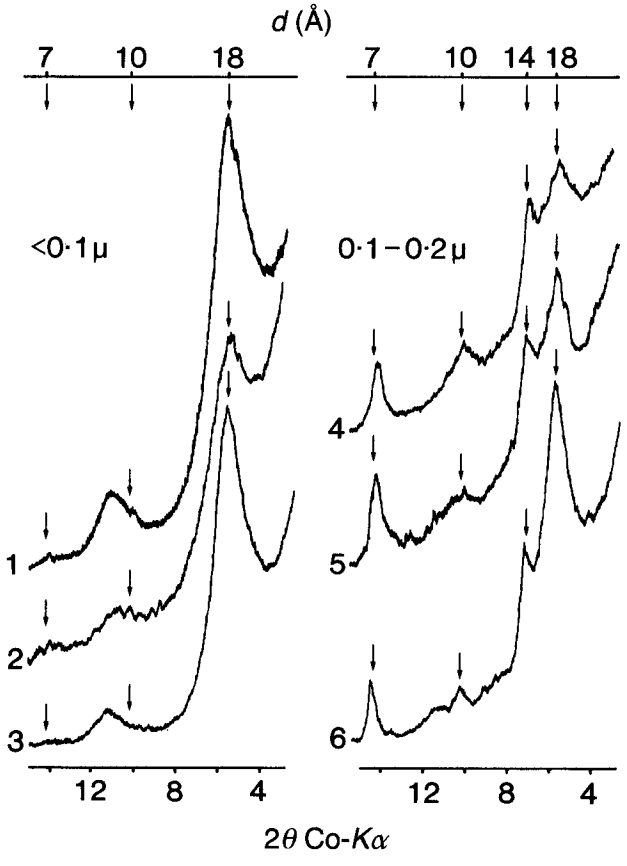

FIG. 1. X-ray powder diffractograms of oriented and glycerol saturated samples.

The relative intensities of all peaks within a diagram change considerably following the Lp correction, higher angle peaks being enhanced relative to those at lower angles. Weakly developed shoulders in the uncorrected diagrams become symmetrical and clearly visible peaks after the corrrection (e.g. the peak at 18 Å in the sample with $n_c = 9$ in Fig. 2). Illite 001, hardly visible in the uncorrected diagrams, changes to a shoulder in most examples. The baseline has been linearized by the correction, thus allowing the application of the fitting program. Even more important is a consistent shift of the peak positions (marked with vertical bars in Fig. 2) to higher angles (i.e. lower d-values). The shifts of the d-values range from 1·0 Å ($n_c = 10$) to 4·5 Å ($n_c = 15$; Fig. 3).

Assuming the strongest peaks in the uncorrected diagrams to originate from vermiculite, linear regression analysis of d_{001} against the chain lengths gave a slope of 1·31 and an $r = 0{\cdot}986$ ($n = 8$). This slope is obviously too high, since a perpendicular orientation of the alkylchains would yield an increase of only 1·27 Å per n_c.

In the corrected diagrams, however, the vermiculite shows distinct second order peaks (002) from $n_c = 11$ to $n_c = 18$ (Fig. 2). These gave a linear regression line of $y = 9{\cdot}02 + 1{\cdot}157x$ ($n = 8$, $r = 0{\cdot}9993$) with $x = n_c$ and $y = d_{002} \times 2$ [Å]. The layer-charge density is $-0{\cdot}88$ Eq per $(Si,Al)_4O_{10}$ unit (= half unit-cell or formula unit = f.u.). This vermiculite

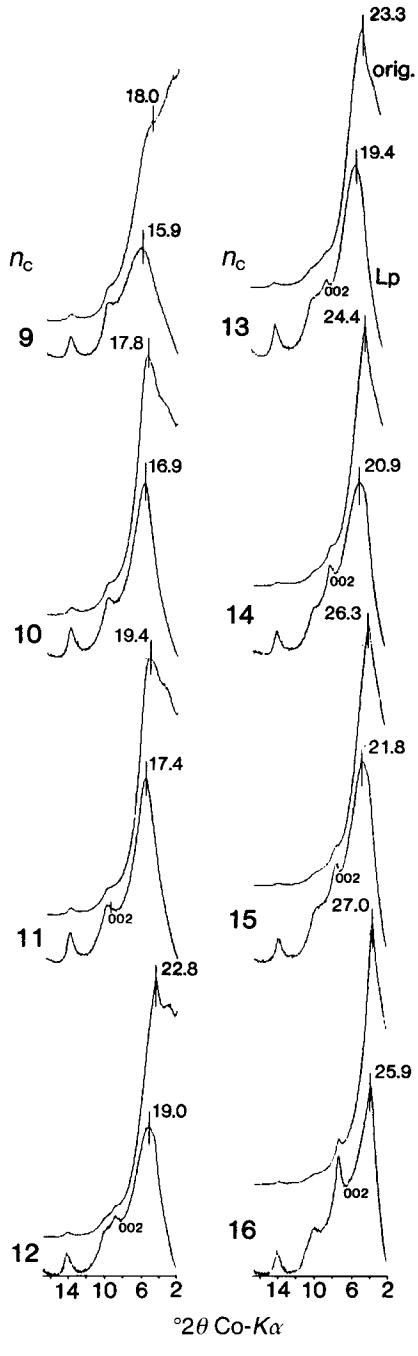

FIG. 2. Uncorrected and Lorentz- and polarization-corrected scans for sample 1 treated with alkylammonium ions from n_c = 9–16. Vertical lines indicate d-values of peak maxima in Å.

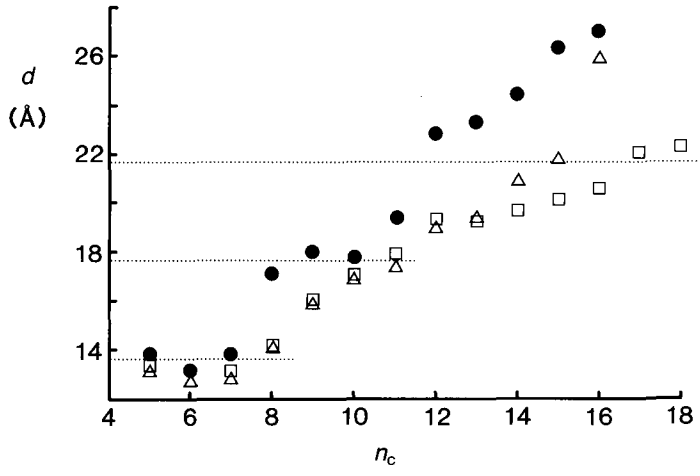

FIG. 3. Basal *d*-values (Å) *vs.* chain length of alkylammonium ions for sample 1. Solid dots = visual inspection of uncorrected data; triangles = visual inspection of Lp-corrected data; squares = Lp-corrected and fitted data. Horizontal lines indicate the *d*-values of the monolayer-, bilayer- and pseudotrimolecular arrangements of the alkylammonium chains.

seems to have a homogeneous charge distribution (charge heterogeneities would lead to non-integral reflex series), which justifies the use of d_{002}.

Fitting the corrected diagrams increased the calculated layer charge values slightly from $-0{\cdot}88$ to $-0{\cdot}92$ per f.u. using d_{002}. In contrast, a layer charge of $-0{\cdot}72$ with significantly broader confidence limits resulted from the calculation using the first order reflections d_{001}.

In both the uncorrected and corrected diagrams for n_c = 4–7, a low-charge component was observed. At n_c = 7 the monolayer was densely packed, giving an upper layer charge limit of $\xi = -0{\cdot}44$ (Fig. 3).

The significant disagreement between the layer charges calculated from the first and the second order peaks of the high-charge component indicates the presence of a further phase overlapping the first-order peaks. A pronounced asymmetry of the broad peaks at ~5° 2θ, visible in the samples n_c = 12 and n_c = 14 (Fig. 4), confirms this. For values of n_c = 12 and greater, the Lp-corrected diagrams were therefore fitted with two peaks in this region, making a reassignment of all peaks necessary. Hence, in all diagrams from n_c = 5 up to n_c = 11 the most intense peak around 17 Å is not due to high and homogeneously-charged vermiculite (as interpreted above), but rather due to high-charge smectite with a heterogeneous charge distribution. Vermiculite *sensu stricto* first becomes visible at n_c = 12, showing both the first- and second-order peak. The intensities of both peaks increase with increasing chain lengths (Fig. 4) and dominate for values of n_c = 16 and greater.

The *d*-values of the low-charge component significantly exceed the plateau at 17·7 Å (Fig. 3), which would be typical for pure smectites (Lagaly & Weiss, 1975). They are, however, still lower than *d*-values of well-crystallized vermiculites with a homogeneous charge distribution (Rühlicke & Niederbudde, 1985; Ghabru *et al.*, 1989). The discontinuous increase from n_c = 14 and the plateau reached at n_c = 17 and n_c = 18 (cf. Fig. 2) are interpreted as a mixed-layering of low-charge smectite (ξ = 0·30) with a high-charge component. The low-charge component contains double layers, whereas the high-charge

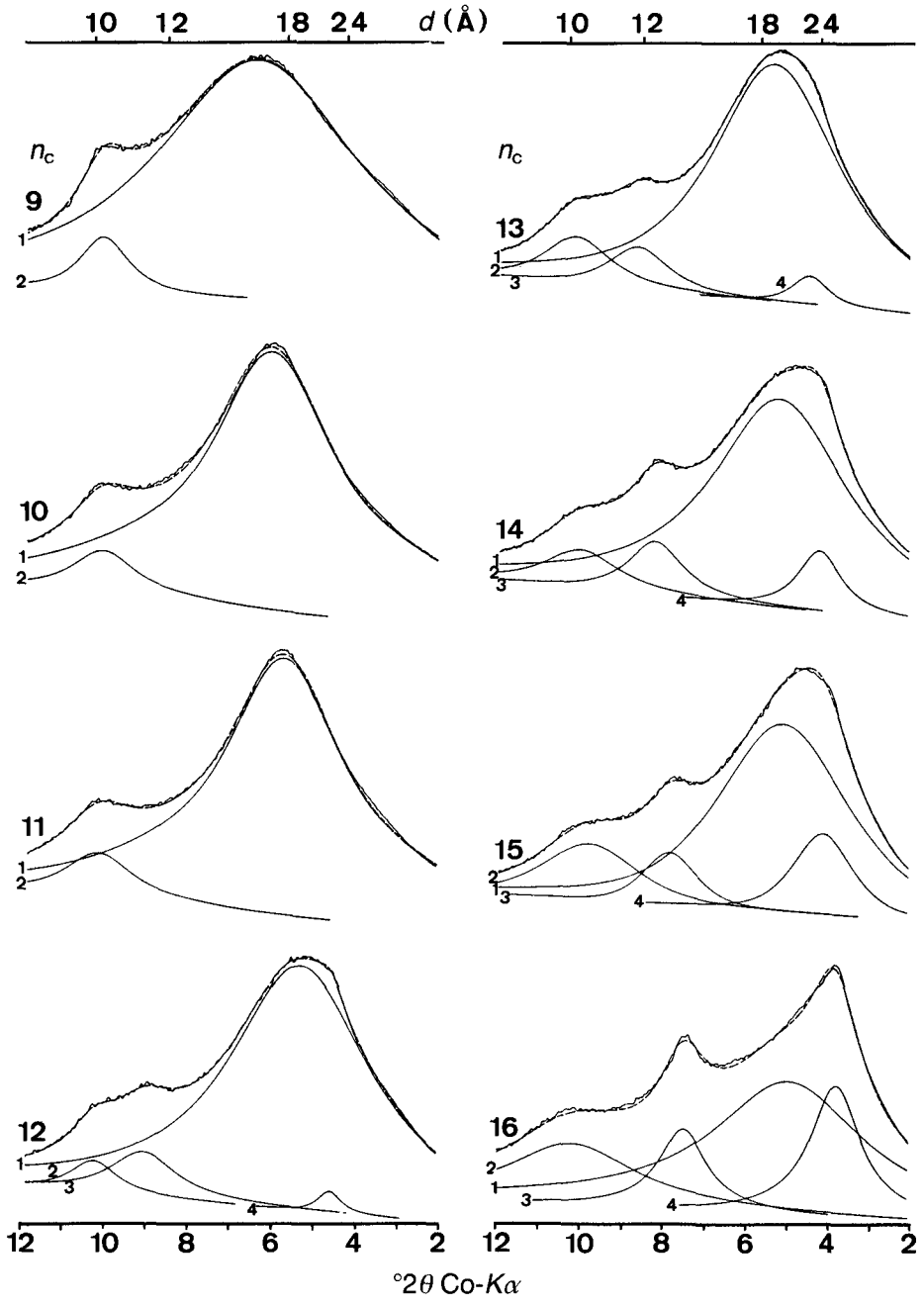

FIG. 4. Lorentz- and polarization-corrected scans for sample 1 treated with n_c = 9–16. Peaks underneath the curves were recalculated from data fits. 1: smectite; 2: illite; 3: vermiculite 002; 4: vermiculite. Dashed line shows the sum of single peaks.

one already contains pseudotrimolecular layers (Lagaly, 1981). Assuming a densely-packed pseudotrimolecular layer at n_c = 17, the high-charge component would have a charge of 0·42 (Lagaly, 1982).

In contrast to the fraction <0·1 μm, the coarser fraction 0·1–0·2 μm of this soil (sample 4) contains more highly charged components (Fig. 5). The asymmetry of the strong peak (pronounced from n_c = 8 up to n_c = 11) again indicates the presence of a further, but minor phase. The second order of the dominant phase, which becomes clearly visible from n_c = 8 and above coincides with 001 of illite at n_c = 9. At n_c = 10 and above, the peak could be resolved from the 001 of illite by the fitting program. Traces of chlorite, visible as a small shoulder at n_c = 8, 9 and 10, do not interfere with the 001 peak of vermiculite (n_c = 16, 17). A further peak that is visible at ~4° 2θ was fitted, but could not be assigned to a specific mineral phase. Lagaly & Weiss (1976) attributed such a peak to X-ray scatter resulting from a superstructure developed in the specimen.

For short chains, the lower plateau of smectite is not developed. The *d*-values of the minor component from n_c = 5 to n_c = 9 are therefore too high for low-charge smectite (cf. sample 4 in Table 2). A linear evaluation of this range yielded a tilting angle of 30° (d = 11·87 ± 0·57 + 0·63 ± 0·08n_c; n = 5, r = 0·997), which is significantly lower than the minimum value of 54° (Lagaly & Weiss, 1969). Gabhru *et al.* (1989) proposed a linear relationship between layer charge and *d*-values for low-charge soil vermiculites derived from oxidized biotites. Assuming the relationship to be valid outside its established range, a layer charge of 0·56 (calculated from 30°) would indicate the transition from a high-charge smectite to a vermiculite of very low charge. This agrees well with the layer charge range of 0·33–0·63, calculated for smectite if the monolayer is assumed to start at n_c = 4. Charge heterogeneities within this phase would give an interstratification of silicate layers with tilted chains and silicate layers containing monolayers of alkylammonium chains. Both

TABLE 2. *d*-values of 001 (Å) of *n*-alkylammonium-treated soil vermiculites (Vm) and smectites (Sm) corrected with internal standard. XRD diagrams were fitted after correction for Lorentz and polarization.

Fraction	<0·1 μm				0·1–0·2 μm					
Sample	2		3		4		5		6	
n_c	Vm	Sm	Vm	Sm	Vm	Vm/Sm*	Vm	Vm/Sm	Vm	Sm
5	–	13·8	–	13·7	16·1	15·1	–	14·3	15·9	13·9
6	–	14·0	–	13·8	17·0	15·6	17·1	14·7	16·6	13·9
7	15·9	14·2	16·2	13·8	17·7	16·2	17·8	15·7	17·9	15·6
8	18·0	14·5	18·1	14·2	18·9	16·9	19·1	16·8	18·9	16·4
9	18·5	16·2	18·8	15·1	20·0	17·6	20·2	17·7	19·7	16·3
10	19·6	17·4	20·9	17·9	20·9	18·1	21·2	18·4	20·3	17·3
11	20·4	17·8	23·7	18·4	22·1	18·5	22·8	18·5	22·6	18·6
12	21·8	17·6	23·5	18·4	23·1	19·4	23·5	19·6	23·4	18·6
13	23·8	17·7	24·3	18·2	24·2	20·7	24·9	19·6	24·5	18·5
14	24·5	18·4	25·7	18·9	25·2	21·2	25·8	21·1	25·4	18·4
15	25·6	19·3	27·6	19·6	26·6	22·2	27·2	22·2	26·9	18·7
16	27·3	19·9	29·4	20·3	28·0	–	28·3	–	28·3	18·9
17	28·5	20·9	30·9	21·2	29·6	–	29·8	–	29·8	19·7

*: *d*-values comprise combination of low-charge vermiculite and high-charge smectite.

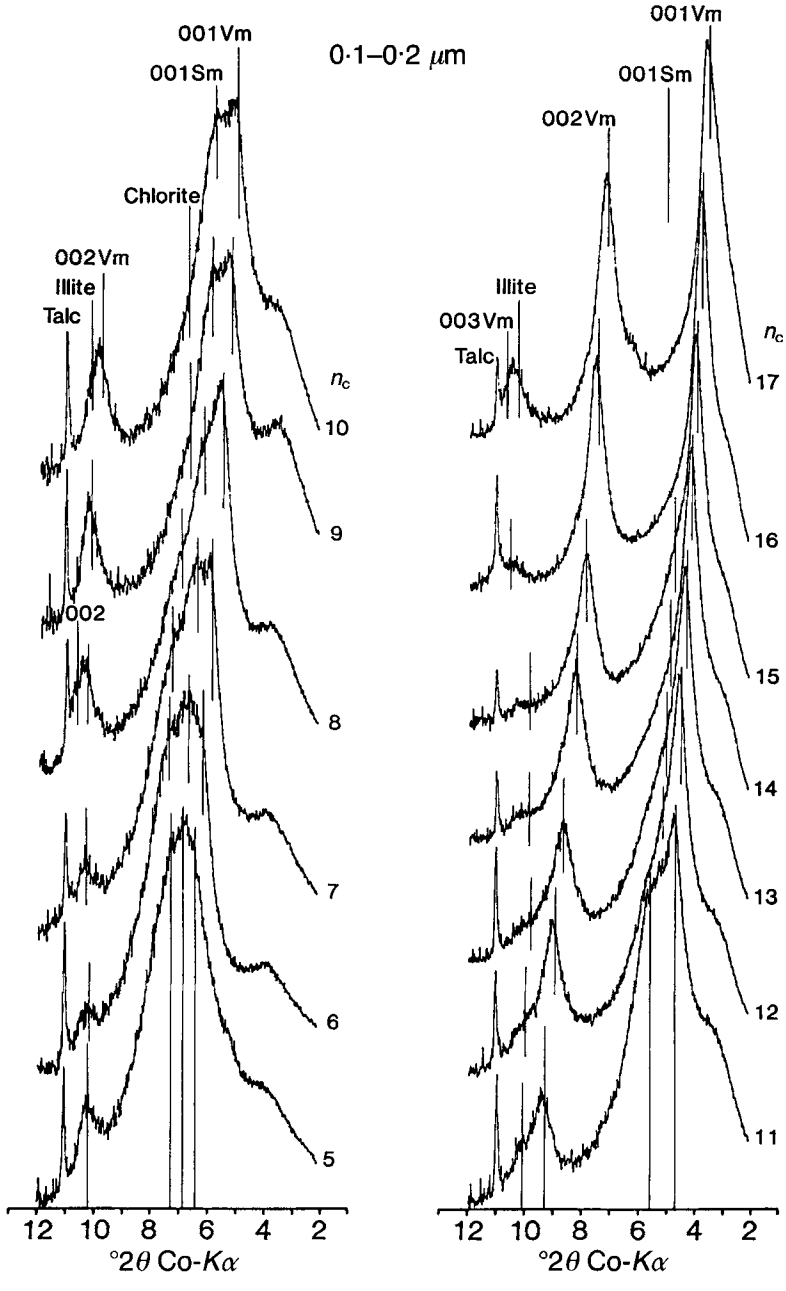

FIG. 5. XRD diagram for sample 4 (0·1–0·2 μm) treated with n_c = 5–11. Vertical bars denote in order of increasing 2θ: 1: Vm 001; 2: Sm 001; 3: Chlorite; 4: Vm 002; 5: Illite; (6: Vm 003). The 001 peak of smectite is visible up to n_c = 15. The strong peak visible at ~4°2θ was fitted, but not used. See text.

different *d*-values would sum up to an average *d*-value intermediate between the "vermiculite" component and the "smectite" component. A further explanation might be the presence of islands of K, which would hamper the full expansion of the sheets with short chains.

Comparison of the fractions <0·1 μm and 0·1–0·2 μm

The mineralogy of sample 2 (<0·1 μm) is dominated by smectite and vermiculite, accompanied by traces of illite (Fig. 6). This was deduced from the pronounced asymmetry of the dominant peak for n_c = 7, 8 and 9, which vanishes with longer chains and becomes visible again at n_c = 12 (cf. Fig. 6). Fitting the diagrams resolved the severe overlap of both smectite and vermiculite peaks, and even allowed a determination of their positions at n_c = 10 and 11 where the asymmetry is absent. A visual evaluation of these diagrams would only have been possible for longer chains (n_c = 13 and higher), where the first order of vermiculite starts to separate from the adjacent smectite peak. The formation of pseudotrimolecular layers starting at n_c = 14 and the absence of a distinct plateau again indicates the smectite to have a high layer charge (Table 2). The layer charge of the vermiculite is not statistically different from 1·0 (ξ = 0·96, ranging from 0·86 to 1·0, r = 0·996). The layer charge of the smectite ranges form 0·32 to 0·54 with a mean value of 0·40.

The mineralogy of the coarser fraction (0·1–0·2 μm) of this soil (sample 5, Fig. 7) is similar to that of sample 4, but the layer charge of smectite is slightly higher. The value of ξ for the vermiculite is 0·89 ± 0·07 (r = 0·999, n = 12) and the layer-charge distribution of the smectite ranges from 0·33 to 0·63 (assuming that the monolayer starts at n_c = 4).

The fractions <0·1 μm and 0·1–0·2 μm of the Humaquept (samples 3 and 6) have higher smectite contents than samples 1 and 4 and samples 2 and 5 (Figs. 8 and 9). The layer-charge distribution of the smectite in the fine clay (<0·1 μm) ranges from 0·32 to 0·48 with a mean charge of 0·38, and is identical to that of the fraction 0·1–0·2 μm (ξ = 0·30–0·48, mean ξ = 0·39). The regression of all 001 *d*-values of vermiculite (sample 3, <0·1 μm) against the chain length gave too high a slope of 1·41 ± 0·14 Å/n_c. The intercept of the regression line was 6·61 ± 1·8 Å. This is unreasonably low, since the theoretical intercept should be 10·34 Å for an NH_4^+ illite (Eugster & Munoz, 1966). Calculating the regression for chains from n_c = 7 to n_c = 14 decreased the slope to 1·34 ± 0·14 and increased the intercept to 7·10 ± 1·51 Å. The *d*-values of n_c = 15, 16 and 17 deviate upwards from the regression line and give the impression of a slight curvature. The too low intercept may be explained either by incomplete expansion with shorter *n*-alkyammonium chains (Rühlicke & Niederbudde, 1985) or by over-proportional expansion at longer chains. With increasing chain length the ability to expand interlayers increases, and therefore higher *d*-values would result. This concept is supported by the fact that an evaluation of the layer charge with single chain lengths and the theoretical intercept yields layer charges well below 1. For n_c = 17, the slope is (30·9–10·34)/17 = 1·21. The reason for the incomplete expansion may be the polarizing effect of K-depleted or alkylammonium-occupied layers on to adjacent layers. Once a single layer is occupied with alkylammonium chains, K in adjacent layers may be bound more strongly. This would be analogous to the K-releasing behaviour of small vermiculite crystals (Bassett, 1959; Scott, 1968; Graf Reichenbach & Rich, 1969).

The coarser fraction contains vermiculite with a homogeneous layer charge of 0·88 ± 0·89.

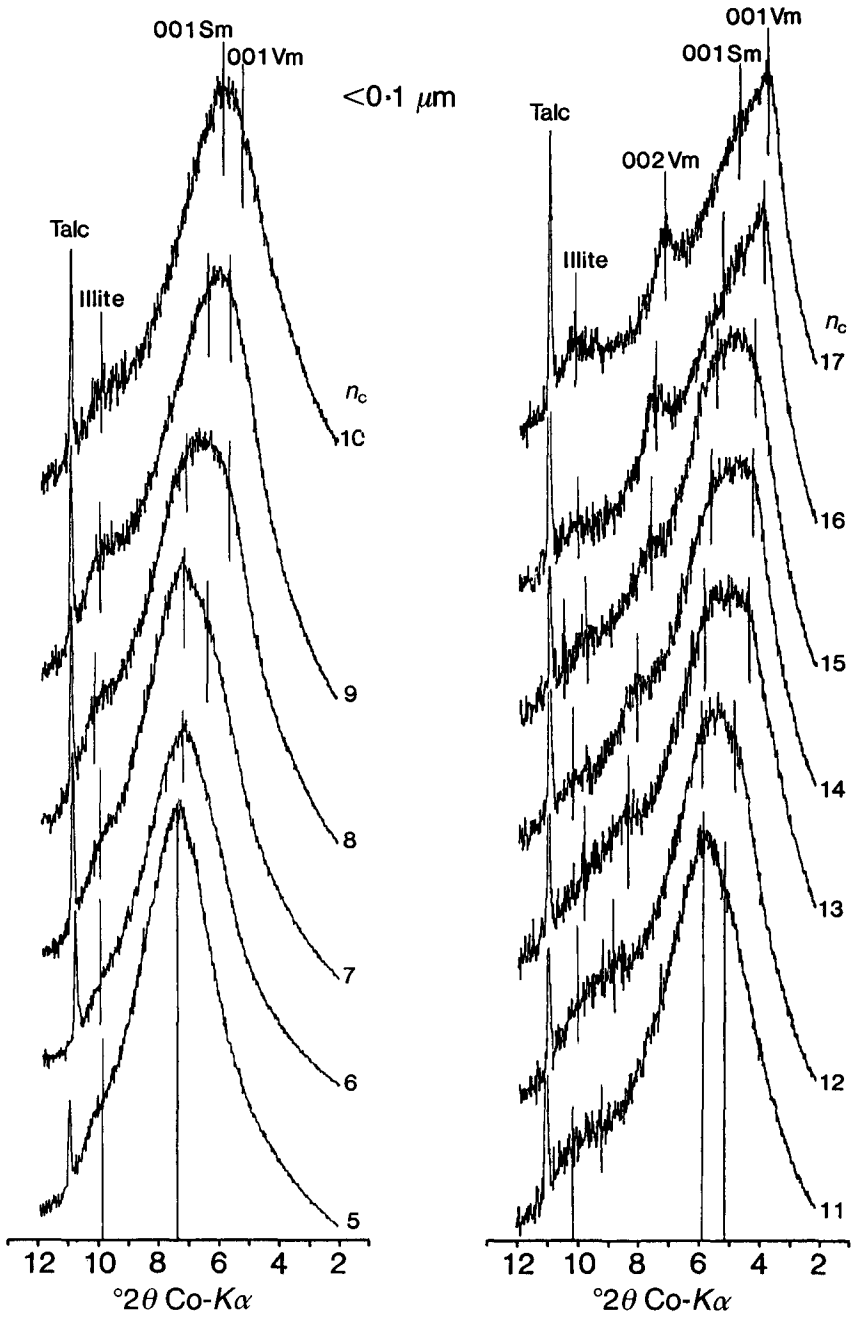

FIG. 6. XRD diagram for sample 2 (<0·1 μm). Vertical bars denote in order of increasing 2θ: 1: Vm 001; 2: Sm 001; 3: Vm 002; 4: Illite. The 001 of vermiculite is visible for n_c = 7 and greater, 002 of vermiculite for n_c = 11 and greater.

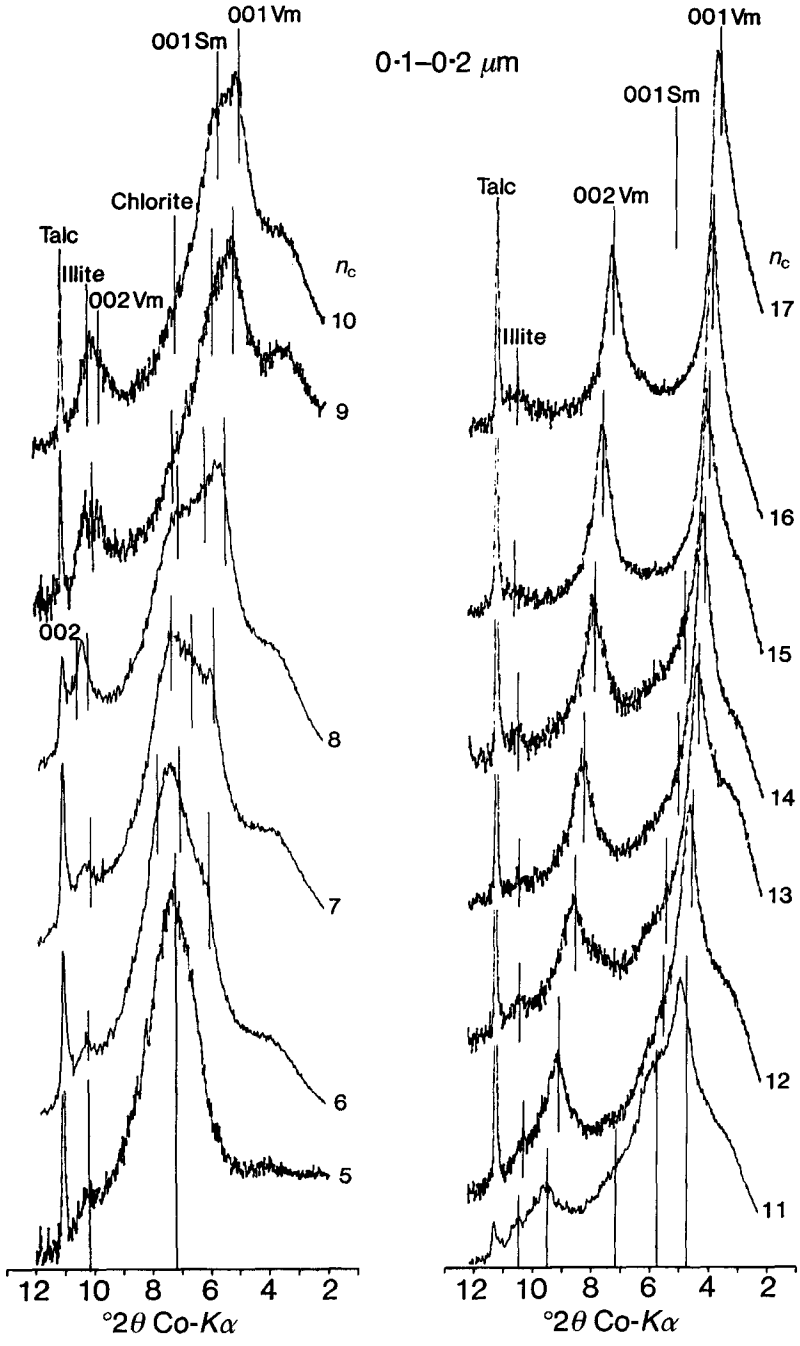

FIG. 7. XRD diagram for sample 5 (0·1–0·2 μm). Vertical bars denote in order of increasing 2θ: 1: Vm 001; 2: Sm 001; 3: Chlorite; 4: Vm 002; 5: Illite. At $n_c = 5$ the peak could not be resolved. Chlorite is visible up to $n_c = 11$.

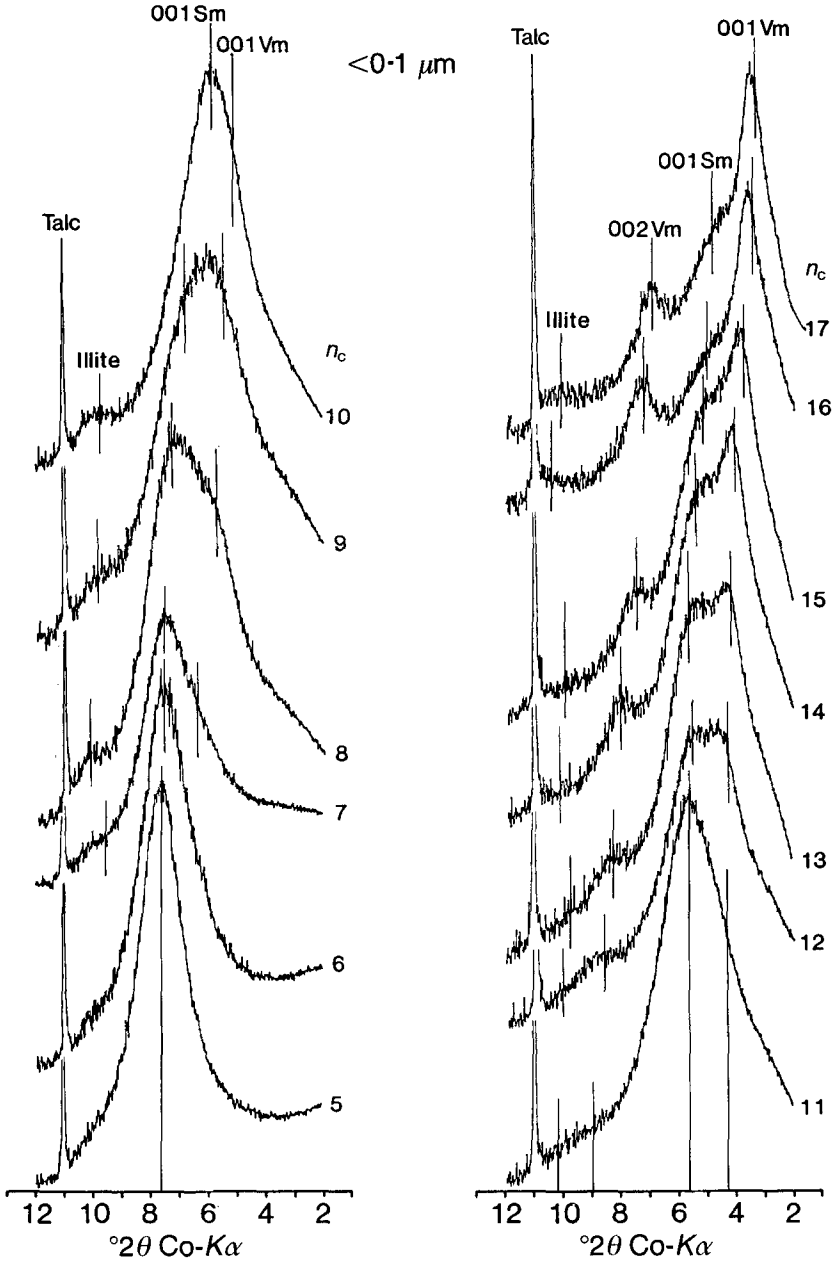

FIG. 8. XRD diagram for sample 3 (<0·1 μm). Vertical bars denote in order of increasing 2θ: 1: Vm 001; 2: Sm 001; 3: Vm 002; 4: Illite. The 001 of vermiculite is visible for n_c = 7 and greater, 002 of vermiculite for n_c = 11 and greater.

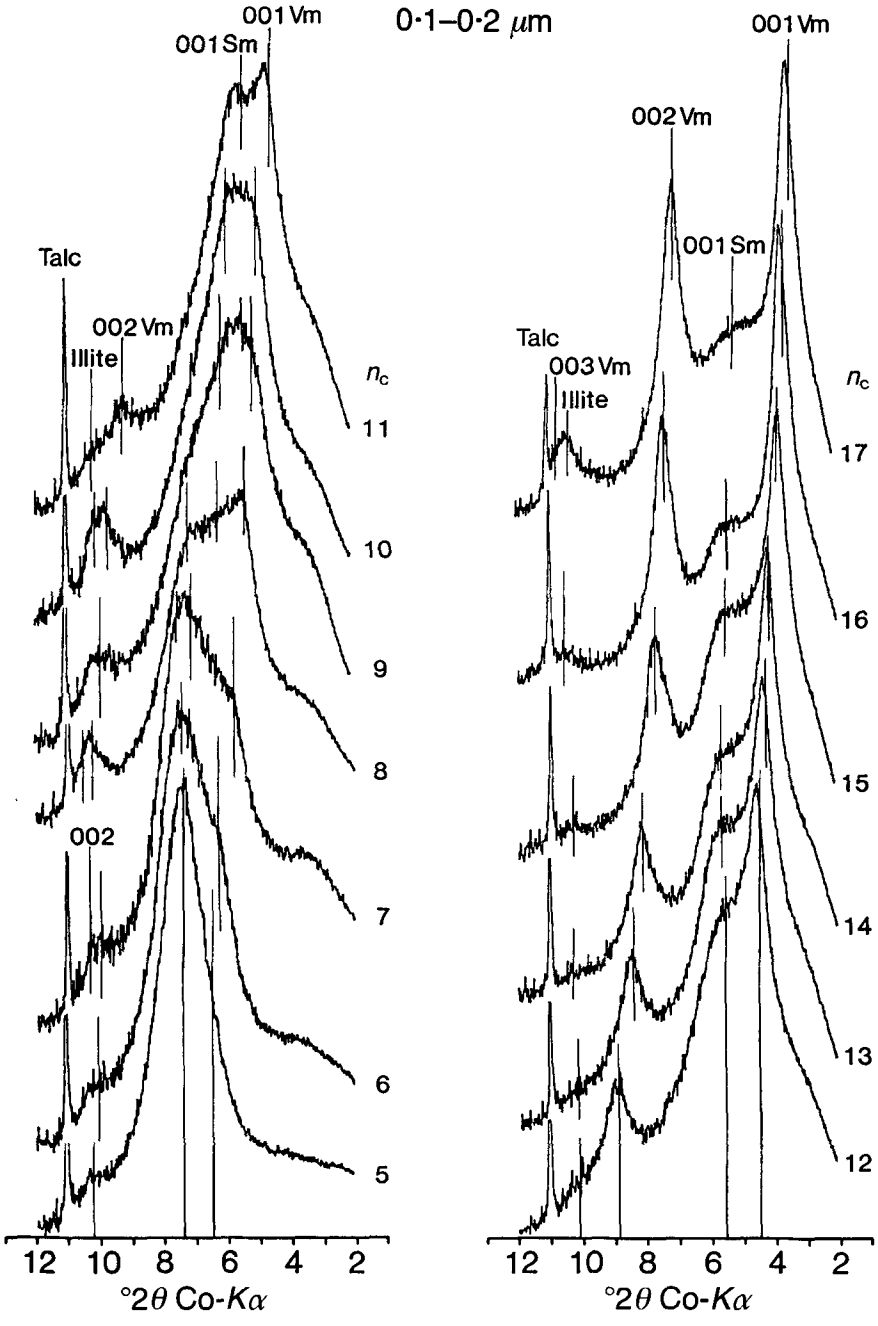

FIG. 9. XRD diagram for sample 4 (0·1–0·2 μm). Vertical bars denote in order of increasing 2θ: 1: Vm 001; 2: Sm 001; 3: Chlorite; 4: Vm 002; 5: Illite; (6: Vm 003). The 001 peak of smectite is visible up to $n_c = 15$.

Potassium release

The K which can be released at $n_c = 18$ (compiled in Table 1) is about twice as high as that which can be released between $n_c = 8$ and $n_c = 10$ (Friedrich, 1985; Niederbudde, 1986; Laird *et al.*, 1987). Compared with the values of Laird *et al.* (1987), the K loss from both soil clay fractions with $n_c = 18$ is very low, but the K release from the 0·1–0·2 μm fraction is higher than that from the smaller fraction (Table 1). This agrees with the observation that illite is more abundant in the coarser fractions. It should not be concluded, however, that high-charge vermiculites are generally produced by release of K from illites. The K depletion of sample no. 3 is less than that of sample no. 2, although the vermiculite content of sample 3 (Fig. 8) is higher than that of sample 2 (Fig. 6) (see the intensities of 001 of vermiculite in Figs. 6 and 8). We conclude, therefore, that well-crystallized vermiculite layers with high charge already exist in the fine clay fraction, although the glycerol-treated sample (no. 3) shows only a broad 18 Å peak.

CONCLUSIONS

The characterization of soil clay minerals is considerably improved by applying a fitting technique to Lp-corrected XRD data of alkylammonium-treated samples. In the soils investigated, the fractions <0·1 μm were dominated by high-charge smectites, whereas the fractions 0·1–0·2 μm contained more high-charge vermiculites. With decreasing particle size, incomplete expansion with alkylammonium chains is likely.

ACKNOWLEDGMENTS

We thank J. Standhaft for analytical work and E. Schuhbauer for preparing all drawings. We also thank two anonymous reviewers for helpful comments. Dr. Murad and M. Jenning kindly improved the English. This research was partly funded by the Deutsche Forschungsgemeinschaft.

REFERENCES

Bassett W.A. (1959) The origin of the vermiculite deposit at Libby. *Am. Miner.* **44,** 282–299.

Beckett P.H.T. (1964) Studies on soil potassium, II. The immediate Q/I relations of labile potassium in the soil. *J. Soil Sci.* **15,** 9–23.

Bish D.L. & Post J.E. (1989) *Modern Powder Diffraction.* (Reviews in Mineralogy, Volume **20**). Mineralogical Society of America, Washington.

Brindley G.W. (1966) Ethylene glycerol and glycol complexes of smectites and vermiculites. *Clay Miner.* **6,** 237–259.

Brindley G.W. (1981) Long-spacing organics for calibrating long spacings of interstratified clay minerals. *Clays Clay Miner.* **29,** 67–68.

Chen C.C., Turner F.T. & Dixon J.B. (1989) Ammonium fixation by high-charge smectite in selected Texas Gulf coast soils. *Soil Sci. Soc. Amer. J.* **53,** 1035–1040.

Eugster H.P. & Munoz J. (1966) Ammonium micas: Possible sources of atmospheric nitrogen. *Science* **151,** 683–686.

Friedrich R. (1985) Schichtladungsbestimmungen und K-Freisetzung mit Alkylammonium an Tonfraktionen aus Lößen und Lößböden. *Mittl. Dtsch. Bodenkundl. Ges.* **43,** 917–922.

Ghabru S.K., Mermut A.R. & Arnaud R.J.St. (1989) Layer-charge and cation-exchange characteristics of vermiculite (weathered biotite) isolated from a gray Luvisol in northeastern Saskatchewan. *Clays Clay Miner.* **37,** 164–172.

Gjems O. (1967) Studies on clay minerals and clay mineral formation on soil profiles in Scandinavia. *Norske Skogfersøksvesen Nr. 81, Vollebekk, Norge,* 301–415.

GRAF VON REICHENBACH H. & RICH C.I. (1969) Potassium release from muscovite as influenced by particle size. *Clays Clay Miner.* **17,** 23–29.

HÄUSLER W. & STANJEK H. (1988) A refined procedure for the determination of the layer charge with alkylammonium ions. *Clay Miner.* **23,** 333–337.

HILBERG DIRK (1989) Akima-Interpolation. *c't Magazin für Computertechnik* 206–214.

JANIK L.M. & RAUPACH M. (1977) An iterative, least-squares program to separate infrared absorption spectra into their component bands. *CSIRO Div. of Soils Tech. Paper* **35,** 1–37.

KLUG H.P. & ALEXANDER L.E. (1973) *X-ray Diffraction Procedures for Polycrystalline and Amorphous Materials.* J. Wiley & Sons, New York.

LAGALY G. (1981) Characterization of clays by organic compounds. *Clay Miner.* **16,** 1–21.

LAGALY G. (1982) Layer charge heterogeneity in vermiculites. *Clays Clay Miner.* **30,** 215–222.

LAGALY G. & WEISS A. (1969) Determination of layer charge in mica-type layer silicates. *Proc. Int. Clay Conf. Tokyo,* **1,** 61–68.

LAGALY G. & WEISS A. (1976) The layer charge of smectitic layer silicates. *Proc. Int. Clay Conf. Mexico,* 157–172.

LAGALY G., FERNANDEZ GONZALES M. & WEISS A. (1976) Problems in layer-charge determination of montmorillonite. *Clay Miner.* **11,** 173–187.

LAIRD D.A., FENTON T.E. & SCOTT A.D. (1988) Layer charge of smectites in an argi alboll-argi aquoll sequence. *Soil Sci. Soc. Amer. J.* **52,** 463–467.

LAIRD D.A., SCOTT A.D. & FENTON T.E. (1987) Evaluation of the alkylammonium method of determining layer charge. *Clays Clay Miner.* **37,** 41–46.

LAIRD D.A., SCOTT A.D. & FENTON T.E. (1989) Interpretation of alkylammonium characterization of soil clays. *Soil Sci. Soc. Amer. J.* **51,** 1659–1663.

LAVES D. & JÄHN G. (1972) Zur quantitativen röntgenographischen Bodenton-Mineralanalyse. *Arch. Acker-, Pflanzenbau Bodenkde.* **16,** 735–739.

MALLA P.B. & DOUGLAS L.A. (1987) Layer charge properties of vermiculites: Tetrahedral vs. octahedral. *Soil Sci. Soc. Amer. J.* **51,** 1362–1366.

MEHRA O.P. & JACKSON M.L. (1960) Iron oxide removal from soils and clays by dithionite-citrate system buffered with sodium bicarbonate. *Clays Clay Miner.* **7,** 317–327.

NIEDERBUDDE E.A. (1986) Factors affecting potassium release and fixation in soils. *Trans. XIII Int. Congr. Soc. Soil Sci. Hamburg,* **VI,** 1155–1167.

NIEDERBUDDE E.A. & KUßMAUL H. (1978) Tonmineraleigenschaften und -Umwandlungen in Parabraunerde-Profilpaaren unter Acker und Wald in Süddeutschland. *Geoderma* **20,** 239–255.

REYNOLDS R.C. (1980) Interstratified clay minerals. Pp. 249–303 in: *Crystal Structures of Clay Minerals and their X-ray Identification* (G. W. Brindley & G. Brown, editors). Mineralogical Society, London.

RÜHLICKE G. & NIEDERBUDDE E.A. (1985) Determination of layer-charge density of expandable 2:1 clay minerals in soils and loess sediments using the alkylammonium method. *Clay Miner.* **20,** 291–300.

SAVITZKY A. & GOLAY M.J.E. (1964) Smoothing and differentiation of data by simplified least squares procedures. *Anal. Chem.* **36,** 1627–1639.

SAVITZKY A. & GOLAY M.J.E. (1972) Comments on smoothing and differentiation of data by simplified least square procedure. *Anal. Chem.* **44,** 1906–1909.

SCHERRER P. (1918) Bestimmung der Größe und der inneren Struktur von Kolloidteilchen mittels Röntgenstrahlen. *Nachr. d. königl. Ges. Wiss. zu Göttingen,* **26,** 98–100.

SCHULZE D.G. (1984) The influence of aluminum on iron oxides VIII. Unit-cell dimension of Al-substituted goethites and estimation of Al from them. *Clays Clay Miner.* **32,** 36–44.

SCOTT A.D. (1968) Effect of particle size on interlayer potassium exchange in micas. *Trans. 9th Int. Congr. Soil. Sci. Adelaide,* **11,** 649–660.

STANJEK H. & FRIEDRICH R. (1986) The determination of layer charge by curve-fitting of Lorentz- and polarization-corrected X-ray diagrams. *Clay Miner.* **21,** 183–190.

WALKER G.F. (1958) Reactions of expanding-lattice clay minerals with glycerol and ethylene glycol. *Clay Miner. Bull.* **3,** 302–313.

WEIR A.H. & RAYNER J.H. (1974) An interstratified illite-smectite from Denchworth series soil in weathered Oxford clay. *Clay Miner.* **10,** 173–187.